ACS APPLIED MATERIALS & INTERFACES

Research Article

www.acsami.org

3,5-Dinitrobenzoic Acid-Capped Upconverting Nanocrystals for the Selective Detection of Melamine

Chanchal Hazra, Venkata N. K. B. Adusumalli, and Venkataramanan Mahalingam*

Department of Chemical Sciences, Indian Institute of Science Education and Research (IISER)-Kolkata, Mohanpur Campus, West Bengal 741252, India

Supporting Information

ABSTRACT: In this Research Article, we report for the first time the use of upconverting nanoparticles to detect melamine up to nanomolar concentration. Detection of melamine is important as it is one of the adulterant in protein rich food products due to its high nitrogen content. In this work, we have shown how the electron deficient 3,5-dinitrobenzoic acid (DNB)-coated Er/Yb-$NaYF_4$ nanocrystals can specifically bind to electron rich melamine and alter the upconverting property of the nanocrystals. This selective binding led to the quenching of the upconversion emission from the nanocrystals. The high selectivity is verified by the addition of various analytes similar in structure with that of melamine. In addition, the selective quenching of the upconversion emission is reversible with the addition of dilute acid. This process has been repeated for more than five cycles with only a slight decrease in the sensing ability. The study was also extended to real milk samples, where the milk adulterated with melamine quenches the emission intensity of the DNB coated $NaYF_4$:Er/Yb nanocrystals, whereas hardly any change is noted for the unadulterated milk sample. The high robustness and the sharp emission peaks make Er^{3+}/Yb^{3+}-doped $NaYF_4$ nanocrystals a potential melamine sensing material over other organic fluorophores and nanocrystals possessing broad emissions.

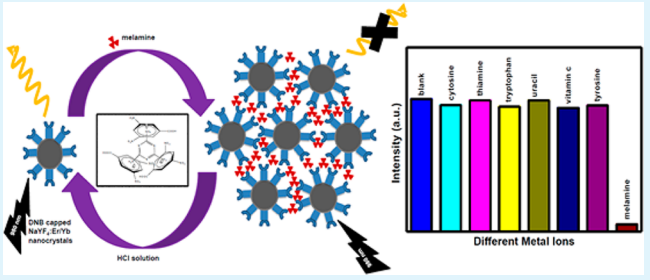

KEYWORDS: *3,5-dintrobenzoic acid, lanthanides, nanocrystals, upconversion, melamine*

INTRODUCTION

Melamine, an organic base and a trimer of cyanamide, with a 1,3,5-triazine skeleton is an important industrial material which had wide application in plastic engineering and agriculture as fertilizer in the early 50s.[1] However, the high nonprotein nitrogen content of melamine led to illegal use in infant formula, wheat gluten, pet foods, etc., to increase the apparent protein content.[2] Standard tests such as the Kjeldahl and Dumas tests[3] used to estimate protein levels in food products by measuring the nitrogen content, can easily be misled by adding nitrogen-rich compounds such as melamine. In 2007, several pet food brands have been recalled in U.S. by Food and Drug Administration (FDA) because of an outbreak melamine-induced illness.[4] The UN food standard commission set the new guidance and safety limit of melamine in food and infant formula as 2.5 and 1 parts-per-million (ppm), respectively.[5,6]

Various analytical methods have been used for the melamine assay. For example, chromatographic techniques become a general method for melamine detection.[7−9] Huang et al. have reported melamine detection in a complex mixture using a low temperature plasma probe-tandem mass spectrometry.[10,11] The detection of melamine in untreated milk and wheat gluten by electrospray ionization mass spectrometry was also demonstrated.[12] Yang and co-workers used chemical ionization mass spectrometric technique for the detection of melamine in milk products.[13] Although these techniques are very sensitive they are quite expensive. On the other hand, nanoparticles are quite robust and can be synthesized easily. There have been only few reports on the use of nanoparticles {NPs} to determine melamine in the recent past.[14−16] For example, hydrogen-bonding based color change in cyanuric acid derivative-grafted gold nanoparticles for visual detection of melamine has been reported.[17,18] Li et al. reported a portable sensor system based on surface-enhanced Raman scattering (SERS) of Au nano-fingers for the detection of trace amounts of melamine in milk products.[19] Lin and co-workers have developed a sensitive turn-on fluorescent detection method for melamine based on FRET between fluorescein and Au NPs.[20] However, to the best of our knowledge, there have been no reports on the use of upconverting nanoparticles for the selective detection of melamine.

Upconverting materials are lanthanides (Ln^{3+})-doped materials which possess the ability to convert low energy near-infrared (NIR) radiation into high-energy visible radiation.[21−31] Recently, there is much interest in upconverting nanomaterials as they find applications in metal ion and chemical sensing,[32,33] bioimaging,[34−38] and enzymatic and affinity assays.[39−41] Furthermore, the luminescent signals of

Received: February 24, 2014
Accepted: April 17, 2014
Published: April 17, 2014

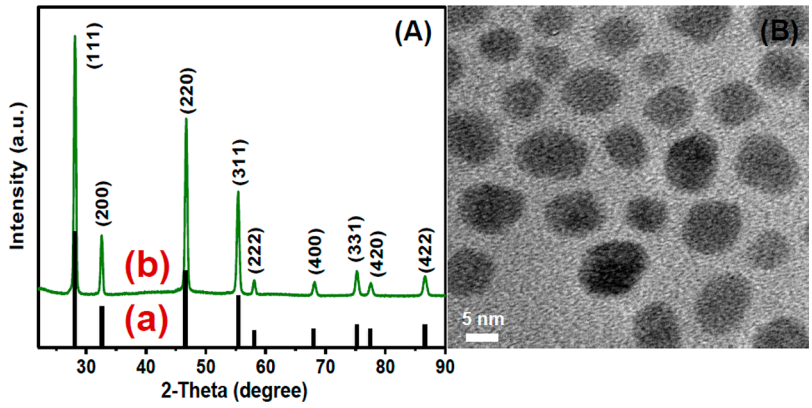

Figure 1. (A) XRD pattern of $NaYF_4$:Er^{3+}/Yb^{3+}nanocrystals (a), standard pattern (b), and (B) TEM image of nanocrystals dispersed in water.

Ln^{3+} ions are quite sharp compared to the broad absorption of gold nanoparticles thus minimizing the interference from other factors like autofluorescence.[42−46]

In this Research Article, we report the use of upconverting nanocrystals for the selective detection of melamine. This is achieved by coating the surface of the nanocrystals with electron deficient groups such as 3,5-dinitrobenzoic acid. Melamine being electron rich is expected to have strong interactions with the DNB-coated nanocrystals. Indeed, addition of melamine selectively quenches the luminescence signals from the upconverting nanocrystals because of the aggregation of the nanocrystals. The high selectivity toward melamine determination is found to be reversible by the addition of HCl, which recovered almost 90% of the initial luminescence intensity.

EXPERIMENTAL SECTION

Materials. Y_2O_3, Er_2O_3, Yb_2O_3 (99.99%, from Aldrich), HNO_3 (1 M, 70%, from Merck), NaF (98%, from Merck), EtOH (Merck), and 3,5-dinitrobenzoic acid (DNB, 97%, from Loba Chemicals) were used for the synthesis. All chemicals were used without further purification.

Synthesis. DNB-coated $NaYF_4$:Yb^{3+}/Er^{3+} nanocrystals were synthesized using a microwave (MW) procedure. Briefly, the stoichiometric amounts of Y_2O_3, Er_2O_3, and Yb_2O_3 were converted into their corresponding nitrate by dissolving in 1 M HNO_3, whereas NaF and DNB were used as received. In a typical procedure, $Y(NO_3)_3$ (0.78 mmol, 298.74 mg), $Yb(NO_3)_3$ (0.20 mmol, 93.4 mg), and $Er(NO_3)_3$ (0.02 mmol, 9.2 mg) were taken in a 100 mL beaker and completely dissolved in 20 mL distilled water. NaF (4 mmol/10 mL 1:1 water−ethanol) was then added as fluoride source, and the solution was stirred vigorously for about 15 min at room temperature. DNB (2 mmol/10 mL H_2O) was slowly added to the solution and stirring was maintained for another 15 min. Subsequently, the colloidal solution was transferred to a 30 mL vial used for microwave synthesis (Anton Parr Monowave 300 microwave reactor under temperature control mode). The vial was tightly sealed with Teflon cap and then microwave heated at 150 °C for 10 min. The final product appeared as precipitate was collected by centrifugation and washed thrice with ethanol, followed by deionized water to remove any unreacted reactants. The XRD patterns were collected using the Rigaku-SmartLab diffractometer attached with D/tex ultra detector and Cu Kα source operating at 35 mA and 70 kV. Scan range was set from 10 to 90° 2θ with a step size of 0.02° with a count time of 2 s. The samples were well powdered and spread evenly on a quartz slide. TEM images were taken on a UHR-FEG-TEM, JEOL; JEM 2100 F model using a 200 kV electron source. Samples were prepared by placing a drop of aqueous dispersion of the nanocrystals on a carbon coated copper grid and the grid was dried under air. Thermogravimetric analysis was performed using Mettler Toledo TGA 851 instrument under N_2 atmosphere at a heating rate of 10 °C min^{-1}. FTIR spectra were collected from a PerkinElmer FT-IR spectrometer 1000 with a resolution of 2 cm^{-1} and averaged over four scans. Upconversion luminescence spectra was done by exciting the 0.01 wt % nanocrystal dispersion with a 980 nm diode laser from RgBLase LLC, which was coupled to a fiber with core diameter of 100 μm. The emitted light was detected using a Horiba JobinYvon fluorimeter equipped with a photomultiplier tube. To remove the scattered excitation light, a long-bandpass filter (495 nm) was used on the excitation side. The size of the NCs was measured by dynamic light scattering (DLS) using a Malvern Zetasizer Nano equipped with a 4.0 mW HeNe laser operating at λ = 633 nm. All samples were measured in a aqueous solution at room temperature with a scattering angle of 173°. Size distribution calculated by Nano software is derived from a non-negative least-squares (NNLS) analysis.

RESULTS AND DISCUSSION

Water dispersible DNB-coated Yb^{3+}/Er^{3+}-doped $NaYF_4$ nanocrystals were successfully synthesized using microwave procedure. Phase analysis of the Yb^{3+}/Er^{3+}-doped $NaYF_4$ nanocrystals was performed using powder X-ray diffraction (PXRD) measurement (see Figure 1A). All diffraction peaks are perfectly matched with the standard pattern of cubic $NaYF_4$ crystals (ICSD PDF Card No.: 01-071-5985). The average size of the nanocrystals is ∼8 nm as evident from TEM image shown in Figure 1B. The high monodispersity in the size is confirmed by the narrow distribution obtained with DLS measurements (vide infra). The average hydrodynamic size of the nanocrystals obtained from the DLS measurements (∼10 nm) is in good agreement with TEM result.

The attachment of DNB molecules onto the surface of the nanocrystals is confirmed by the appearance of strong carbonyl stretching near 1645 cm^{-1} in the FTIR spectrum. This frequency is much lower than that observed for the free DNB molecules. The DNB binding makes the nanocrystals surface hydrophilic thus render them water dispersible. The other stretching vibrations observed near 1540 and 1350 cm^{-1} correspond to the asymmetric and symmetric stretching of nitro groups. The FTIR spectra of the nanocrystals together with that of pure DNB are shown in Supporting Information Figure S1.The DNB coating was further verified with TGA analysis. For the free DNB, the major weight loss is observed from 180 to 300 °C because of the decomposition of the DNB molecules, whereas for the DNB-coated nanocrystals, the onset of decomposition is shifted to 310 °C. This strongly suggests that the DNB molecules are attached to the $NaYF_4$ surface. TGA curves for both free DNB and the DNB coated nanocrystals are shown in Supporting Information Figure S2.

Figure 2 shows the upconversion (UC) emission spectrum of DNB coated $NaYF_4$:Yb^{3+}/Er^{3+} nanocrystals obtained by

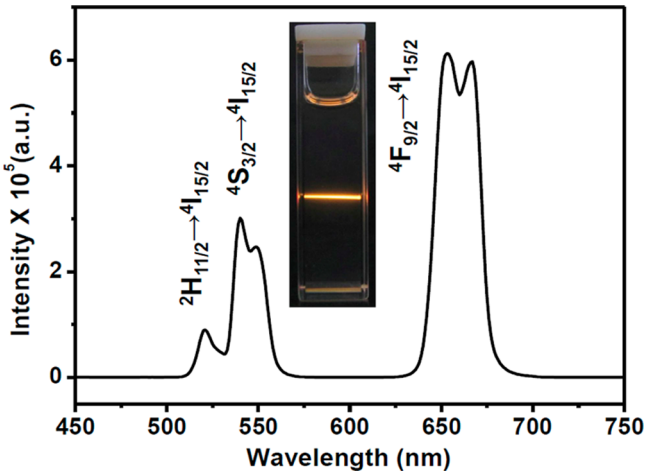

Figure 2. Upconversion (UC) emission spectrum of DNB-capped $NaYF_4$:Er^{3+}/Yb^{3+}nanocrystals in H_2O.

exciting under 980 nm laser. Strong green and red emissions are observed near 550 and 650 nm, respectively. These emissions are ascribed to the $^2H_{11/2}$, $^4S_{3/2} \rightarrow {}^4I_{15/2}$, and $^4F_{9/2} \rightarrow {}^4I_{15/2}$ transitions, respectively. The origin of these emissions is from the excited energy levels of Er^{3+} ions, which are predominantly populated by multiple energy transfers from excited Yb^{3+} ions. The Yb^{3+} ions act as sensitizer for the Er^{3+} ions because of its high absorption coefficient. The number of photons involved in the energy transfer process is understood by doing the power dependent studies as the laser power, $P \alpha I^n$, where I is the intensity of the UC emission and n is the number of photons involved in producing the upconversion emission. The value of n is obtained from the graph of log plot of the laser power against the emission intensity. As shown in Supporting Information Figures S3 and S4 the slopes (n) obtained after fitting the straight lines are 1.73 and 1.70, respectively, for the green and red emission suggesting the involvement of two photons. On the basis of the calculated n values, we propose a mechanism for the upconversion process which is illustrated in Supporting Information Figure S5.

To investigate the sensing ability of the Er^{3+}/Yb^{3+}-doped $NaYF_4$nanocrystals toward melamine solution, aqueous solution of melamine was added to the nanocrystals dispersion. The emission spectra shown in Figure 3 clearly indicate that upon addition of melamine solution, the Er^{3+} emission intensity of the nanocrystals decreases dramatically. To verify the selectivity, Er^{3+}/Yb^{3+}-doped $NaYF_4$ nanocrystals were exposed to the distinct aqueous solution of other similar analytes, such as tyrosine, cytosine, thiamine, uracil, tryptophan, and vitamin C. The UC emission spectra shown in Figure 3 clearly indicate that hardly any change in the emission intensity upon addition of these analytes. The bar diagram in the inset shows the selective quenching of Er^{3+} luminescence intensity occurs only with the addition of melamine. The high selectivity of Er^{3+}/Yb^{3+}-doped $NaYF_4$ nanocrystals toward melamine is verified by measuring the Er^{3+} luminescence from the Er^{3+}/Yb^{3+}-doped nanocrystals dispersion containing both melamine and other analytes. The aqueous solution of each foreign analytes was first added to the dispersion followed by the same concentration of melamine. Figure 4 shows that the Er^{3+} emission intensity from

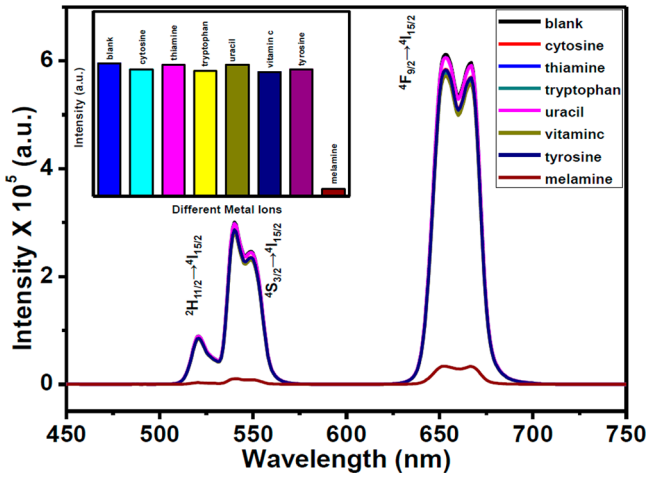

Figure 3. Emission spectra of Er^{3+}/Yb^{3+}-doped $NaYF_4$ nanocrystals after mixing with different analytes including melamine. The inset shows a bar diagram indicating the selective quenching of the luminescence intensity of Er^{3+} ions upon melamine addition.

the nanocrystals is selectively reduced only upon addition of melamine.

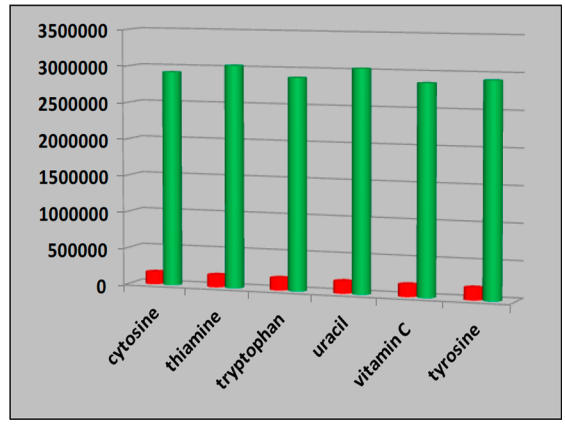

Figure 4. Bar diagram indicating the selective quenching of the UC emission intensity of Er^{3+}/Yb^{3+}-doped $NaYF_4$ nanocrystals by melamine in the presence of other analytes.

The dinitro aromatics, as an electron acceptor, can favorably interact with electron donors such as primary amines. In the present case, the electron-rich amine groups of melamine have a strong charge transfer (CT) interaction with the electron deficient aromatic nucleus of DNB attached to the surface of the nanocrystals. In addition, hydrogen bonding interaction between O atom ($-NO_2$ groups of DNB) and H atom ($-NH_2$ groups of melamine) is also favorable. Such interactions essentially decrease the interparticle distance between the nanocrystals and bring the nanocrystals close together resulting in the formation of aggregation. We presume such strong interaction between the DNB and melamine weakens the interaction between the DNB and the nanocrystal surface. This might lead to the surface defect states which will act as luminescence quenching centers. In addition, the interface between the nanocrystals might act as grain boundaries leading to increase in the nonradiative interactions. The formation of aggregation is supported by DLS as well as TEM images. Figure

dx.doi.org/10.1021/am5011089 | ACS Appl. Mater. Interfaces 2014, 6, 7833−7839

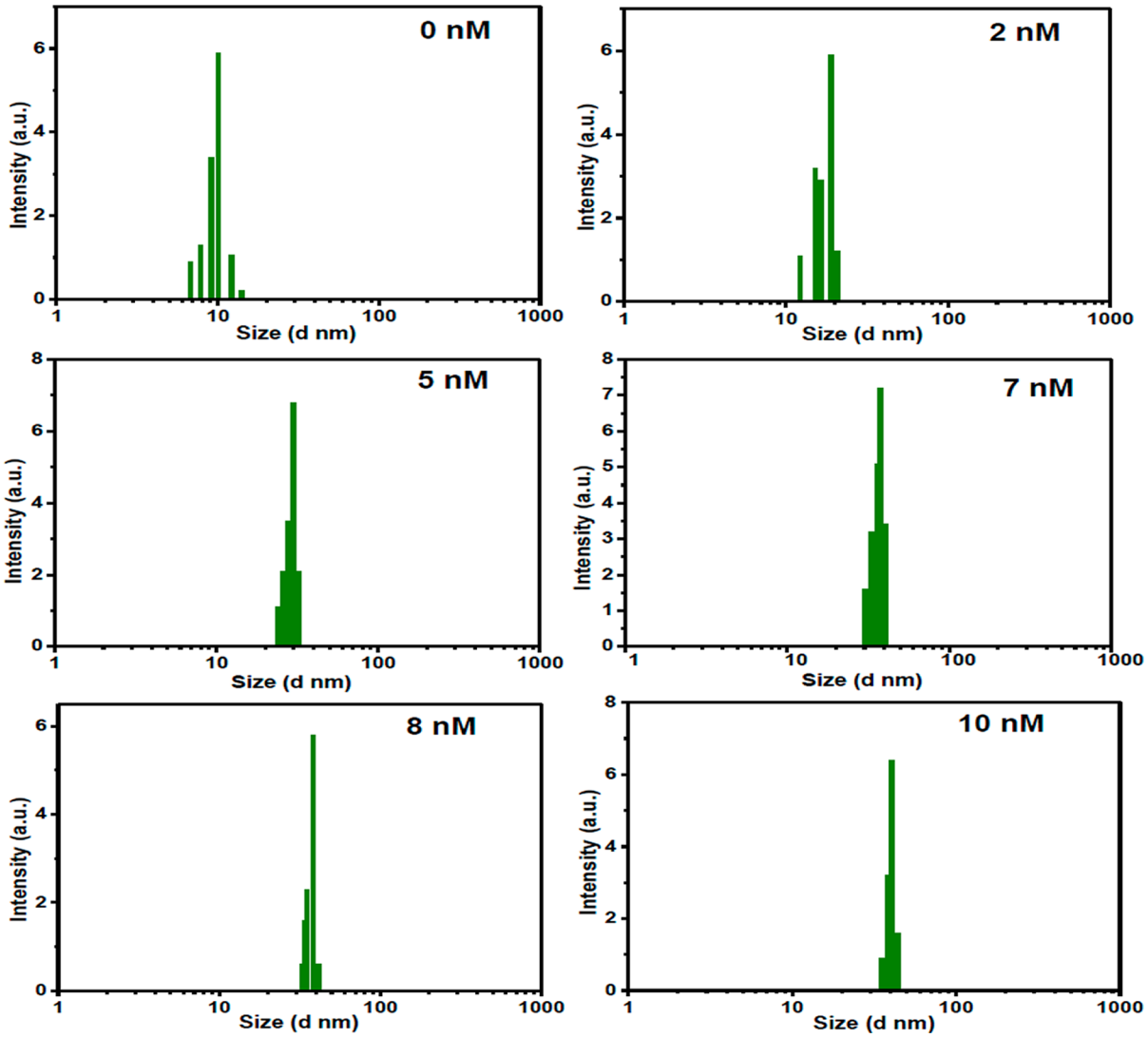

Figure 5. Snap shots of the size distribution of DNB coated Er^{3+}/Yb^{3+}-doped $NaYF_4$ nanocrystals after addition of different concentration of melamine.

5 shows the DLS results indicating an increase in the average particle size with the addition of melamine.

Similarly in TEM images increased aggregation of nanocrystals is observed for 10 nM melamine addition compared to 2 nM sample (see Supporting Information Figure S6). The proposed mechanism is further supported by the absence of any change in the average particle size of DNB-capped $NaYF_4$ nanocrystals with the addition of other analytes. The DLS results for the same are shown in Supporting Information Figure S7. A schematic of the proposed mechanism is shown in Figure 6.

We believe that hydrogen bonding or CT interactions between the nitro groups of DNB and amino groups of melamine may lead to weakening of nanocrystal−DNB interaction. This might lead to development of some surface defects, thereby the emission intensity of the Er^{3+} ions present near the surface of the nanocrystals is quenched. To verify this we have prepared a series of $NaYF_4$ nanocrystals with 0.5, 1, and 2 mol % Er^{3+} concentrations. The luminescence studies of all the samples were performed with the addition of 10 nM melamine to the nanocrystals dispersion. These samples are again found to be very selective toward melamine. However, for the 2 mol % sample the decrease in the emission intensity upon melamine addition is 95% which is greater than 80% and 55% observed for 1 mol % and 0.5 mol % samples, respectively (shown in Figure 7). It is reasonable to assume that in the 2 mol % sample more Er^{3+} ions reside near the surface of the nanocrystals compared to the 1 mol % samples, and 0.5 mol %.

To verify whether the selective quenching of luminescence by melamine is reversible, we titrated the melamine complexed $NaYF_4$:Er^{3+}/Yb^{3+} with 0.1 M HCl. Upon addition of HCl, there is a gradual increase in the Er^{3+} luminescence suggesting that the nature of the complexation is reversible. It is clear from Figure 7, that more than 90% of the initial intensity is recovered. We presume this is due to the formation of melamine: HCl adduct. This cycle can be done multiple times with only a decrease in the luminescence intensity (see inset in Figure 8).

To understand whether the quenching process is collisional (dynamic) in nature we performed concentration dependence study (i.e., Stern−Volmer plot) which is shown in Supporting Information Figure S8. The plot of I_0/I against the melamine concentration is almost linear suggesting that the quenching may be either dynamic or static in nature. To verify further we

dx.doi.org/10.1021/am5011089 | ACS Appl. Mater. Interfaces 2014, 6, 7833−7839

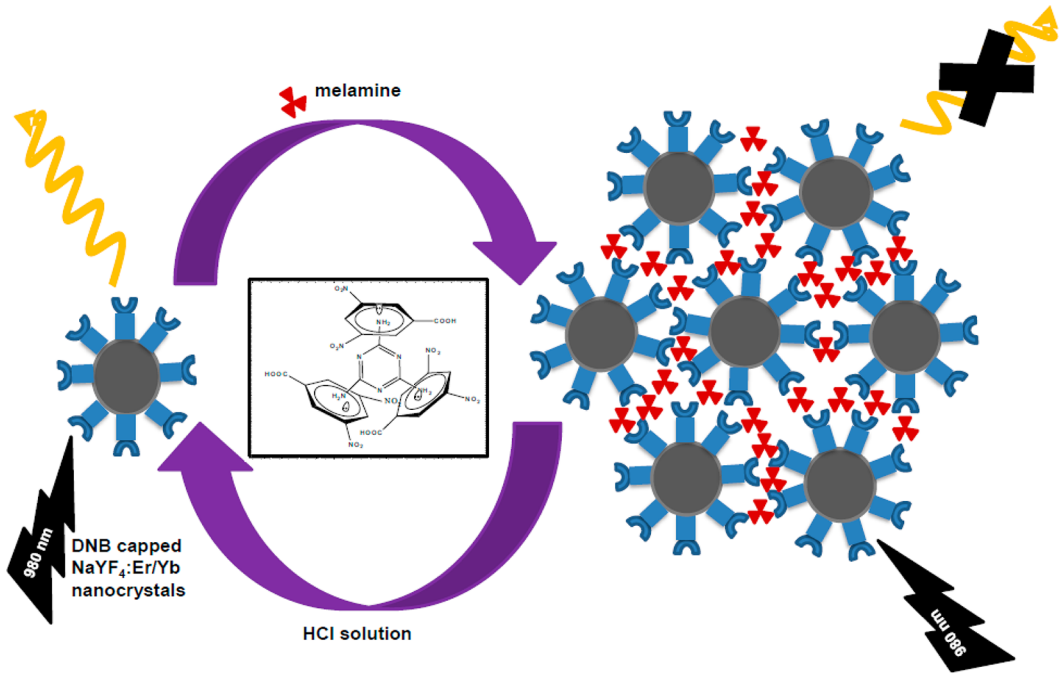

Figure 6. Scheme illustrating the interaction of melamine with DNB capped $NaYF_4:Er^{3+}/Yb^{3+}$ nanocrystals.

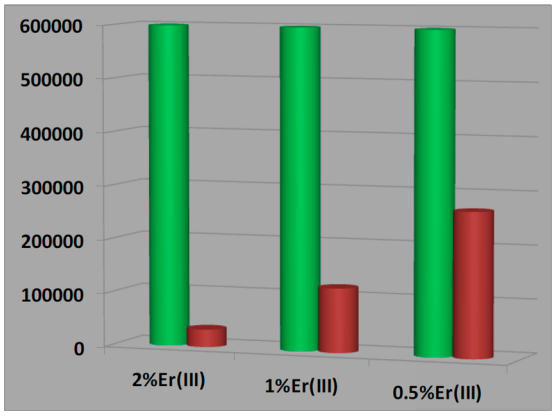

Figure 7. Graph showing the larger decrease in the emission intensity for 2 mol % Er^{3+} in Er/Yb-doped $NaYF_4$ NCs compared to 0.5% and 1 mol % nanocrystals samples upon addition of melamine solution to each.

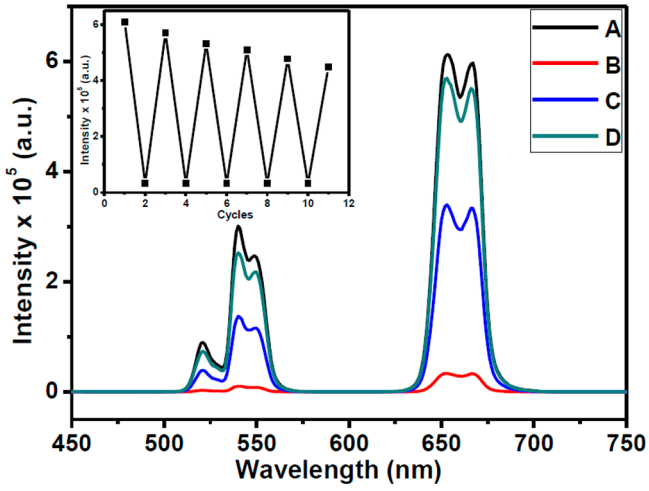

Figure 8. UC emission spectra of melamine complexed-Er^{3+}/Yb^{3+}-doped $NaYF_4$ nanocrystals after the gradual addition of HCl. (A) luminescence of Er^{3+}/Yb^{3+}-doped $NaYF_4$ nanocrystals (B) after addition of 10 nM melamine (C) after addition of 0.01 (M) HCl and (D) 0.1 (M) HCl. Inset shows luminescence quenching and recovery cycles upon addition of melamine and dilute HCl to the DNB coated nanocrystals.

have performed lifetime measurements. The lifetime of the $^4S_{3/2}$ level of the Er^{3+} ions in DNB-capped Er^{3+}/Yb^{3+}-doped nanocrystals is about 109 μs. This value gradually decreased to 43.5 μs after the addition of 7 nM melamine. The decrease in the lifetime of the Er ions clearly suggests that the quenching of the upconversion emission is dynamic in nature. The lifetime decay curves are shown in Figure 9.

The sensitivity of the $NaYF_4:Yb^{3+}/Er^{3+}$nanocrystals is evaluated using the formula $3\sigma/k$ and is found to be 2.5 (nM) for the melamine determination, where σ is the standard deviation of the blank measurements (n = 7), k is the slope of the linear calibration curve. For comparison, the linear range and detection limit (LOD) obtained from our method are listed in Table S1 (shown in the Supporting Information) along with the corresponding values obtained from other methods, such as SERS and FRET. It is clear from the data that the melamine detection via upconversion method is comparable to other methods.

To understand the suitability of the method to detect melamine in real milk samples; we mixed 5−9 nM concentration of melamine to commercially available milk. The melamine adulterated milk was added to the DNB-coated $NaYF_4$:Er/Yb nanocrystals and the upconversion luminescence was measured. A gradual decrease in the emission intensity of Er^{3+} is observed for the melamine adulterated milk whereas hardly any change in the luminescence intensity is noted for the pure milk sample. This clearly suggests the feasibility of the developed method for the detection of melamine in the nanomolar regime. The results are shown in Supporting Information Figure S9. A linear relationship is observed between the luminescence intensity of $NaYF_4:Er^{3+}/Yb^{3+}$

dx.doi.org/10.1021/am5011089 | ACS Appl. Mater. Interfaces 2014, 6, 7833−7839

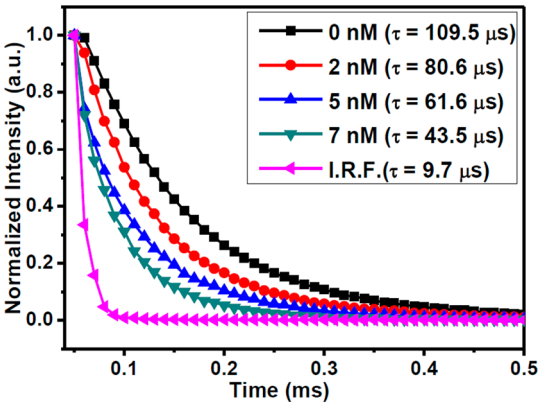

Figure 9. Lifetime decay curves of DNB capped Er^{3+}/Yb^{3+}-doped NaYF4 nanocrystals measured by monitoring the 550 nm emission.

nanocrystals and the concentration of melamine in the range of 5×10^{-9}–1×10^{-7} (M) in the melamine-mixed milk samples. The sensitivity of the $NaYF_4:Yb^{3+}/Er^{3+}$nanocrystals is evaluated using the formula $3\sigma/k$ and is found to be 9.1 (nM) for the melamine determination, where σ is the standard deviation of the blank measurements (n = 5), k is the slope of the linear calibration curve. To check the feasibility of this method over melamine detection, we calculated % recovery and RSD for samples with different melamine concentration (5–100 nM) and the values are shown in Table S2 in the Supporting Information. For comparative purpose the linear range, detection limit (LOD), % recovery, RSD, etc., of our method are listed in Table S3 (Supporting Information) along with other conventional mass spectrometric or chromatographic methods. It is clear that the present method provided a comparable detection limit, dynamic range, % recovery and RSD values to the other reported methods for melamine detection in real samples (milk). The calibration curve for real sample analysis is given in the inset in Figure S9 in the Supporting Information.

CONCLUSION

Water dispersible 3,5-dinitrobenzoic acid capped $NaYF_4:Yb^{3+}/Er^{3+}$ nanocrystals were prepared by microwave procedure. Upon 980 nm excitation, the nanocrystals show strong upconversion emissions near 550 and 650 nm, whose intensities were selectively quenched upon addition of melamine. This luminescence quenching is very selective as addition of similar analytes like tyrosine, cytosine, etc. hardly affected the intensity of the UC emission. Moreover, the detection of melamine was found to be reversible with the addition of 0.1 M HCl. More than 90% of the initial intensity of the Er^{3+} was recovered upon HCl addition. We believe, our findings opens a new avenue for the detection of melamine up to 2.5 nM level, which is well below the safety limit set by UN food Standard Commission. We strongly believe that the present detection method may be advantageous over other methods because $NaYF_4:Er^{3+}/Yb^{3+}$ nanocrystals are quite robust and display two emission bands in the visible spectrum and their large anti-Stokes shift allows for an easy separation of the emission peaks from the excitation light source (i.e., 980 nm). In addition, they display narrow emission bands with longer luminescence lifetimes, which can be an additional tool to follow the sensing. Finally, the 980 nm diode lasers are very cheap and are available as laser pointers, which are easy to carry anywhere.

ASSOCIATED CONTENT

Supporting Information

Experimental, IR, TGA, UC power dependence study, UC mechanism, DLS, Stern–Volmer plot, UC spectra of melamine-tainted milk samples, and tables showing data comparison with other methods. This material is available free of charge via the Internet at http://pubs.acs.org.

AUTHOR INFORMATION

Corresponding Author

*Fax: 91-33-25873020. Tel: +91(0)9007603474. E-mail: mvenkataramanan@yahoo.com.

Notes

The authors declare no competing financial interest.

ACKNOWLEDGMENTS

V.M. thanks the Department of Science and Technology (DST) India, CSIR and IISER-Kolkata for the funding. C.H. and V.N.K.B.A. thank IISER-Kolkata and UGC, respectively, for their scholarship.

REFERENCES

(1) Wei, F.; Lam, R.; Cheng, S.; Lu, S.; Ho, D.; Li, N. Rapid Detection of Melamine in Whole Milk Mediated by Unmodified Gold Nanoparticles. *Appl. Phys. Lett.* **2010**, *96*, No. 133702.

(2) Chen, X.; Hu, Y.; Gao, J.; Zhang, Y.; Li, S. Interaction of Melamine Molecules with Silver Nanoparticles Explored by Surface-Enhanced Raman Scattering and Density Functional Theory Calculations. *Appl. Spectrosc.* **2013**, *67*, 491–497.

(3) Cohen. J. B. *Practical Organic Chemistry*, 2nd ed; MacMillan: London, 1910.

(4) http://www.fda.gov/Animal/Veterinary/SafetyHealth/RecallsWithdrawals/ucm129575.htm (accessed on 11 December 2012).

(5) Ai, K.; Liu, Y.; Lu, L. Hydrogen-Bonding Recognition-Induced Color Change of Gold Nanoparticles for Visual Detection of Melamine in Raw Milk and Infant Formula. *J. Am. Chem. Soc.* **2009**, *131*, 9496–9497.

(6) Zhao, B.; Liu, Z. R.; Liu, Z. L.; Liu, G. X.; Li, Z.; Wang, J. X.; Dong, X. T. Silver Microspheres for Application as Hydrogen Peroxide Sensor. *Electrochem. Commun.* **2009**, *11*, 1707–1710.

(7) Yokley, R. A.; Mayer, L. C.; Rezaaiyan, R.; Manuli, M. E.; Cheung, M. W. Analytical Method for the Determination of Cyromazine and Melamine Residues in Soil Using LC-UV and GC-MSD. *J. Agric. Food Chem.* **2000**, *48*, 3352–3358.

(8) Ihunegbo, F. N.; Tesfalidet, S.; Jiang, W. Determination of Melamine in Milk Powder Using Zwitterionic HILIC Stationary Phase with UV Detection. *J. Sep. Sci.* **2010**, *33*, 988–995.

(9) Ping, H.; Zhang, M.; Li, H.; Li, S.; Chen, Q.; Sun, C.; Zhang, T. Visual Detection of Melamine in Raw Milk by Label-Free Silver Nanoparticles. *Food Control* **2012**, *23*, 191–197.

(10) Huang, G.; Ouyang, Z.; Cooks, R. G. High-Throughput Trace Melamine Analysis in Complex Mixtures. *Chem. Commun.* **2009**, 556–558.

(11) Huang, G.; Xu, W.; Visbal-Onufrak, M. A.; Ouyang, Z.; Cooks, R. G. Direct Analysis of Melamine in Complex Matrices Using a Handheld Mass Spectrometer. *Analyst* **2010**, *135*, 705–711.

(12) Zhu, L.; Gamez, G.; Chen, H.; Chingin, K.; Zenobi, R. Rapid Detection of Melamine in Untreated Milk and Wheat Gluten by Ultrasound-Assisted Extractive Electrospray Ionization Mass Spectrometry (EESI-MS). *Chem. Commun.* **2009**, 559.

(13) Yang, S. P.; Chen, H. W.; Yang, Y. L.; Hu, B.; Zhang, X.; Zhou, Y. F.; zhang, L. L.; Gu, H. W. Imaging Melamine in Egg Samples by

Surface Desorption Atmospheric Pressure Chemical Ionization Mass Spectrometry. *Chin. J. Anal. Chem.* **2009**, *37*, 315.
(14) Ping, H.; Zhang, M.; Li, H.; Li, S.; Chen, Q.; Sun, C.; Zhang, T. Visual Detection of Melamine in Raw Milk by Label-Free Silver Nanoparticles. *Food Control* **2012**, *23*, 191−197.
(15) Chen, X.; Hu, Y.; Gao, J.; Zhang, Y.; Li, S. Interaction of Melamine Molecules with Silver Nanoparticles Explored by Surface-Enhanced Raman Scattering and Density Functional Theory Calculations. *Appl. Spectrosc.* **2013**, *67*, 491−497.
(16) Gao, F.; Ye, Q.; Qui, P.; Zhang, L. Efficient Fluorescence Energy Transfer System between CdTe-Doped Silica Nanoparticles and Gold Nanoparticles for Turn-On Fluorescence Detection of Melamine. *J. Agric. Food Chem.* **2012**, *60*, 4550−4558.
(17) Li, N.; Wei, F.; Lam, R.; Zou, J.; Cheng, S.; Lu, S.; Ho, D. Gold Nanoparticle-Mediated Detection of Melamine Based on a Dual Colorimetric and Turbidometric Readouts. *IEEE Int. Conf. Nanotechnol, 10th* **2010**, 736−739.
(18) Seto, C. T.; Whitesides, G. M. Self-Assembly Based on the Cyanuric Acid-Melamine Lattice. *J. Am. Chem. Soc.* **1990**, *112*, 6409−6411.
(19) Kim, A.; Barcelo, S. J.; Williams, R. S.; Li, Z. Melamine Sensing in Milk Products by Using Surface Enhanced Raman Scattering. *Anal. Chem.* **2012**, *84*, 9303−9309.
(20) Guo, L.; Zhong, J.; Wu, J.; Fu, F. F.; Chen, G.; Chen, Y.; Zheng, X.; Lin, S. Sensitive Turn-on Fluorescent Detection of Melamine Based on Fluorescence Resonance Energy Transfer. *Analyst* **2011**, *136*, 1659−1663.
(21) Auzel, F. Upconversion and Anti-Stokes Processes with f and d Ions in Solids. *Chem. Rev.* **2004**, *104*, 139−173.
(22) Wang, H. Q.; Nann, T. Monodisperse Upconverting Nanocrystals by Microwave-Assisted Synthesis. *ACS Nano* **2009**, *3*, 3804−3808.
(23) Sarkar, S.; Messaragandla, B.; Hazra, C.; Mahalingam, V. Sub-5 nm Ln^{3+}-doped $BaLuF_5$ Nanocrystals: A Platform to Realize Upconversion via Interparticle Energy Transfer (IPET). *Adv. Mater.* **2013**, *25*, 856−860.
(24) Rahman, P.; Green, M. The Synthesis of Rare Earth Fluoride Based Nanoparticles. *Nanoscale* **2009**, *1*, 214−224.
(25) Heer, S.; Kompe, K.; Haase, M.; Güdel, H. U. Highly Efficient Multicolour Upconversion Emission in Transparent Colloids of Lanthanide-Doped $NaYF_4$ Nanocrystals. *Adv. Mater.* **2004**, *16*, 2102−2105.
(26) Pedroni, M.; Piccinelli, F.; Passuello, T.; Polizzi, S.; Ueda, J.; Gonzalez, P. H.; Maestro, L. M.; Jaque, D.; Solé, J. G.; Bettinelli, M.; Speghini, A. Water (H_2O and D_2O) Dispersible NIR-to-NIR Upconverting Yb^{3+}/Tm^{3+} Doped MF_2 (M = Ca, Sr) Colloids: Influence of the Host Crystal. *Cryst. Growth Des.* **2013**, *13*, 4906−4913.
(27) Wang, F.; Han, Y.; Lim, C. S.; Lu, Y.; Wang, J.; Xu, J.; Chen, H.; Zhang, C.; Hong, M.; Liu, X. Simultaneous Phase and Size Control of Upconversion Nanocrystals through Lanthanide Doping. *Nature* **2010**, *463*, 1061−1065.
(28) Sivakumar, S.; Veggel, F. C. J. M. van.; May, P. S. Near-Infrared (NIR) to Red and Green Up-Conversion Emission from Silica Sol-Gel Thin Films Made with $La_{0.45}Yb_{0.50}Er_{0.05}F_3$ Nanoparticles, Hetero-Looping-Enhanced Energy Transfer (Hetero-LEET): A New Up-Conversion. *J. Am. Chem. Soc.* **2007**, *129*, 620−625.
(29) Ehlert, O.; Thomann, R.; Darbandi, M.; Nann, T. A Four-Color Colloidal Multiplexing Nanoparticle System. *ACS Nano* **2008**, *2*, 120−124.
(30) Mader, H. S.; Kele, P.; Saleh, S. M.; Wolfbeis, O. S. Upconverting Luminescent Nanoparticles for Use in Bioconjugation and Bioimaging. *Curr. Opin. Chem. Biol.* **2010**, *14*, 582−596.
(31) Wang, L.; Yan, R. X.; Huo, Z. Y.; Wang, L.; Zeng, J. H.; Bao, J.; Wang, X.; Peng, Q.; Li, Y. Fluorescence Resonant Energy Transfer Biosensor Based on Upconversion-Luminescent Nanoparticles. *Angew. Chem., Int. Ed.* **2005**, *44*, 6054−6057.
(32) Saleh, S. M.; Ali, R.; Wolfbeis, O. S. Quenching of the Luminescence of Upconverting Luminescent Nanoparticles by Heavy Metal Ions. *Chem.—Eur. J.* **2011**, *17*, 14611−14617.
(33) Achatz, D. E.; Ali, R.; Wolfbeis, O. S. Luminescent Chemical Sensing, Biosensing, and Screening Using Upconverting Nanoparticles. *Top. Curr. Chem.* **2011**, *300*, 29−50.
(34) Wang, F.; Banerjee, D.; Liu, Y.; Chen, X.; Liu, X. Upconversion Nanoparticles in Biological Labeling, Imaging, and Therapy. *Analyst* **2010**, *135*, 1839−1854.
(35) Pichaandi, J.; Boyer, J. C.; Delaney, K. R.; Veggel, F. C. J. M. van. Two-Photon Upconversion Laser (Scanning and Wide-Field) Microscopy Using Ln^{3+}-Doped $NaYF_4$ Upconverting Nanocrystals: A Critical Evaluation of their Performance and Potential in Bioimaging. *J. Phys. Chem. C* **2011**, *115*, 19054−19064.
(36) van Veggel, F. C. J. M.; Dong, C.; Johnson, N. J. J.; Pichaandi, J. Ln^{3+}-Doped Nanoparticles for Upconversion and Magnetic Resonance Imaging: Some Critical Notes on Recent Progress and Some Aspects to be Considered. *Nanoscale* **2012**, *4*, 7309−7321.
(37) Nyk, M.; Kumar, R.; Ohulchanskyy, T. Y.; Bergey, E. J.; Prasad, P. N. High Contrast in Vitro and in Vivo Photoluminescence Bioimaging Using Near Infrared to Near Infrared Up-Conversion in Tm^{3+}- and Yb^{3+}-Doped Fluoride Nanophosphors. *Nano Lett.* **2008**, *8*, 3834−3838.
(38) Chatterjee, D. K.; Gnanasammandhan, M. K.; Zhang, Y. Small Upconverting Fluorescent Nanoparticles for Biomedical Applications. *Small* **2010**, *6*, 2781−2795.
(39) Bünzli, J. C. G.; Eliseeva, S. V. Lanthanide NIR Luminescence for Telecommunications, Bioanalyses and Solar Energy Conversion. *J. Rare Earths* **2010**, *28*, 824−842.
(40) Rantanen, T.; Jarvenpaa, M. L.; Vuojola, J.; Kuningas, K.; Soukka, T. Fluorescence-Quenching-Based Enzyme−Activity Assay by Using Photon Upconversion. *Angew. Chem., Int. Ed.* **2008**, *47*, 3811−3813.
(41) Sivakumar, S.; Diamente, P. R.; Veggel, F. C. J. M. van. Silica-Coated Ln^{3+}-Doped LaF_3 Nanoparticlesas Robust Down and Upconverting Biolabels. *Chem.—Eur. J.* **2006**, *12*, 5878−5884.
(42) Blasse. G.; Grabmaier. B. C. *Luminescent Materials*, 1st ed.; Springer Verlag: Berlin, 1994.
(43) Bünzli, J-C. G.; Eliseeva, S. V. Intriguing Aspects of Lanthanide Luminescence. *Chem. Sci.* **2013**, *4*, 1939−1949.
(44) Bünzli, J-C. G.; Piguet, C. Lanthanide-Containing Molecular and Supramolecular Polymetallic Functional Assemblies. *Chem. Rev.* **2002**, *102*, 1897−1928.
(45) Dorenbos, P. Electronic Structure Engineering of Lanthanide Activated Materials. *J. Mater. Chem.* **2012**, *22*, 22344−22349.
(46) Montini, T.; Speghini, A.; Rogatis, L.; De Lorenzut, B.; Bettinelli, M.; Graziani, M.; Fornasiero, P. Identification of the Structural Phases of $Ce_xZr_{1-x}O^2$ by Eu(III) Luminescence Studies. *J. Am. Chem. Soc.* **2009**, *131*, 13155−13160.